Cancer Research

Anti–PD-L1 Treatment Results in Functional Remodeling of the Macrophage Compartment

Huizhong Xiong[1], Stephanie Mittman[1], Ryan Rodriguez[1], Marina Moskalenko[1], Patricia Pacheco-Sanchez[1], Yagai Yang[1], Dorothee Nickles[2], and Rafael Cubas[1]

Abstract

Checkpoint inhibitors like anti-PD1/PD-L1 have demonstrated significant therapeutic efficacy in a subset of patients partly through reinvigoration of CD8 T cells. However, their impact on myeloid cells remains largely unknown. Here, we report that anti–PD-L1 treatment favorably impacts the phenotype and function of tumor macrophages by polarizing the macrophage compartment toward a more proinflammatory phenotype. This phenotype was characterized by a decrease in Arginase-I (ARG1) expression and an increase in iNOS, MHCII, and CD40 expression. Whole-transcriptome profiling further confirmed extensive polarization of both tumor monocytes and macrophages from a suppressive to a proinflammatory, immunostimulatory phenotype. This polarization was driven mainly through IFNγ and was associated with enhanced T-cell activity. Transfer of monocytes into anti–PD-L1–treated tumor-bearing mice led to macrophage differentiation into a more proinflammatory phenotype, with an increase in CD8 T cells expressing granzyme-B and an increase in the CD8/Treg ratio compared with control-treated mice. Although in responsive tumor models, anti–PD-L1 treatment remodeled the macrophage compartment with beneficial effects on T cells, both macrophage reprogramming and depletion were needed to maximize anti–PD-L1 responses in a tumor immune contexture with high macrophage burden. Our results demonstrate that anti–PD-L1 treatment can favorably remodel the macrophage compartment in responsive tumor models toward a more proinflammatory phenotype, mainly through increased IFNγ levels. They also suggest that directly targeting these cells with reprogramming and depleting agents may further augment the breadth and depth of response to anti–PD-L1 treatment in less responsive or more macrophage-dense tumor microenvironments.

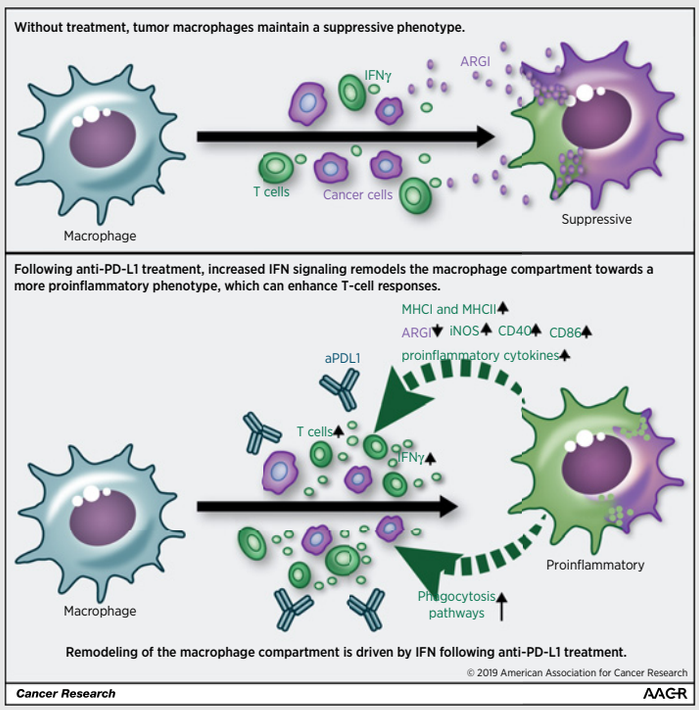

Significance: This work demonstrates that increased IFNγ signaling following anti–PD-L1 treatment can remodel the macrophage compartment to enhance T-cell responses.

Graphical Abstract: http://cancerres.aacrjournals.org/content/canres/79/7/1493/F1.large.jpg.

[1]Department of Translational Oncology, Genentech, South San Francisco, California. [2]Bioinformatics and Computational Biology, Genentech, South San Francisco, California.

Note: Supplementary data for this article are available at Cancer Research Online (http://cancerres.aacrjournals.org/).

Corresponding Author: Rafael Cubas, Genentech, 1 DNA Way MS-50, South San Francisco, CA 94080. Phone: 650-225-1539; Fax: 650-225-1411; E-mail: cubasr@gene.com

doi: 10.1158/0008-5472.CAN-18-3208

Introduction

Tumor-associated macrophages (TAM) are abundantly found in tumors and contribute critically to the immune set point (1–3). The activation state of macrophages is generally characterized as M1 (classic) and M2 (alternative; refs. 4, 5). M1 macrophages are mannose receptor low ($CD206^{low}$), express high levels of MHCII ($MHCII^{high}$), and are characterized by high expression of inducible nitric oxide synthase (iNOS), as well as costimulatory molecules like CD40, CD86, and various proinflammatory cytokines (6). M2 macrophages, on the other hand, are $CD206^{high}$ $MHCII^{low}$, and release anti-inflammatory and immunosuppressive mediators such as Arginase-I (ARG1), IL10, and TGFβ (7).

In the cancer setting, TAMs display remarkable heterogeneity and plasticity (1, 2, 4). The definition of M1 and M2, derived from *in vitro* polarization assays, lies at two extremes and is often considered inaccurate for describing the complexity of TAM functional states *in vivo*. Thus, in our work, we refer to TAMs as either M1-like, M1/M2 intermediate, or M2-like to reflect different degrees of mixed phenotypes within this spectrum (2, 8). M1-like macrophages have been positively associated with overall survival (OS) in a variety of human cancers, whereas M2-like macrophages are poor prognostic indicators (9). Recent studies have shed light on the complexity of macrophage function. Fcγ receptors and IL1β have been reported to be involved in phagocytosis-induced PDL1 and IDO expression (10), and iNOS has been shown to play both anti- and protumoral roles (11–13) despite continuing to serve as a common M1-associated marker (14–16). These results highlight the necessity to examine the expression of multiple markers and to integrate whole transcriptome analysis for a more accurate evaluation of macrophage functional state.

Given the importance of macrophages as major immune modulators in the tumor microenvironment, macrophage-targeting strategies are under intense investigation with two main approaches: depletion and repolarization (17, 18). Various depleting agents that block monocyte recruitment and/or TAM differentiation are currently being tested (2). Repolarization of macrophages aims at changing the phenotype of TAMs from an immune-suppressive to an immune-stimulatory state. Properly educated TAMs can have notable beneficial characteristics, expressing high levels of MHC, costimulatory molecules, secreting proinflammatory cytokines, and actively killing antibody-opsonized cancer cells through phagocytosis (19, 20). Repolarized TAMs could therefore become efficient antigen-presenting cells activating CD8 and CD4 T cells *in situ* (21). TAM repolarization strategies include agonistic anti-CD40 (aCD40), blockade of CSF1 signaling, selective inhibition of PI3Kγ, deletion of *Dicer*, as well as targeting surface markers expressed by suppressive macrophages (2, 8, 16, 21–28). Repolarization and depletion have recently been combined to achieve an optimal stimulatory phenotype on macrophages; however, its implication on tumor sensitization to checkpoint inhibitors remains unclear (27).

Checkpoint inhibitors like anti-PD1/PD-L1 (aPD1/PDL1) and anti-CTLA4 (aCTLA4) have proven effective and durable in a subset of patients in a variety of cancers (29–31). Extensive work has mainly focused on exploring T-cell functionality and their reinvigoration mechanisms following treatment (3, 32–36). Despite numerous efforts at understanding the mechanism of action of checkpoint inhibitors and macrophage polarization, little is known about the connection between the two. A recent study demonstrated profound remodeling of monocyte and macrophage subsets after aPD1/aCTLA4 treatment, with an increase in iNOS and a decrease in CD206 expression, which was partially dependent on IFNγ (37). These results suggest that TAMs can actively respond to microenvironment changes mediated by checkpoint blockade and thus should be considered in the design of combinatorial strategies.

Here, we demonstrate that PDL1 blockade in responsive tumor models led to an overall remodeling of the macrophage compartment toward a more proinflammatory phenotype, an effect that was observed in both monocytes and recently differentiated macrophages. We further demonstrate that macrophage polarization following aPDL1 treatment can beneficially impact T-cell responses and that differential manipulation of macrophages based on the tumor immune contexture can be used to significantly augment the activity of aPDL1.

Materials and Methods

Animal study oversight

All animal studies were reviewed and approved by Genentech's Institutional Animal Care and Use Committee. Mice whose tumors exceeded acceptable size limits (2,000 mm^3) or became ulcerated were euthanized and removed from the study.

Mice

Eight– to 10-week-old female C57BL/6 or Balb/c mice were obtained from Charles River Laboratories. The mice were housed at Genentech in standard rodent microisolator cages and were acclimated to study conditions for at least 3 days before tumor cell implantation. Animals were 8- to 10-week-old with an average weight of 19.68 g. Only animals that appeared to be healthy and free of obvious abnormalities were used for the study.

Cell lines

The murine colon adenocarcinoma MC38 cell line was obtained from former GNE colleague Rink Offringa and murine mammary carcinoma EMT6 and JC cell lines were obtained from ATCC, tested for *Mycoplasma* using MycoAlert Mycoplasma Detection Kit (Lonza), kept at low passage and maintained in complete RPMI1640 medium (HyClone) supplemented with 10% heat-inactivated premium grade FBS (VWR) and 2.05 mmol/L L-glutamine.

Syngeneic tumor studies

Tumor cells were harvested in log-phase growth and resuspended in HBSS-containing Matrigel (BD Biosciences) at a 1:1 ratio. For MC38, cells were implanted subcutaneously in the right unilateral thoracic area of C57BL/6 mice at 0.1×10^6 MC38 cells in 100 μL. For EMT6 and JC studies, Balb/c mice were inoculated in the left mammary fat pad #5 with 0.1×10^6 cells in 100 μL. Tumors were monitored until they became established and reached a mean tumor volume of approximately 190 mm^3. Mice with tumors in the range of 130 to 250 mm^3 were then randomized into treatment groups. Treatment was initiated the next day with either isotype (gp120) or aPDL1 (clone 6E11) antibodies given at 10 mg/kg i.v. for the first dose followed by 5 mg/kg i.p., thereafter twice a week for 3 weeks (for efficacy studies). When indicated, anti-mouse IFNγ rat IgG1 (BioXCell, clone: XMG1.2) was administered at 250 μg in 100 μL PBS intraperitoneally, twice a week. In the corresponding studies aCD40 (FGK45) was dosed intraperitoneally once at 4 mg/kg and aCSF1R (2G2) was dosed at

30 mg/kg i.v. once. For tumor volume and body weight measurements, see Supplementary Methods.

Adoptive monocyte transfer

Bone marrows from CD45.1 mice (The Jackson Laboratory, stock no. 002014) were harvested and monocytes were purified using Miltenyi Monocyte Isolation Kit (BM; catalog no. 130-100-629). A total of 2×10^6 monocytes were injected intravenously into the tail vein of each MC38-tumor–bearing CD45.2 recipient mice. Isotype or aPDL1 antibodies were administered 5 days prior to cell transfer. Two days later, tumors were collected and digested for staining and FACS analysis. Monocytes and macrophages were distinguished by Ly6C and F4/80 staining.

Flow cytometry

To generate single-cell suspensions, tumors were collected, cut into 2–4 mm pieces, and digested for 30 minutes using the murine Tumor Dissociation Kit from Miltenyi (Miltenyi Biotec) following the manufacturer's instructions (catalog no. 130-096-730). Tumor homogenates were filtered through a 70-μm nylon filter (Corning) and washed twice with RPMI1640 media. After the last wash, cells were resuspended in staining buffer (PBS + 0.5% FCS + 5 mmol/L EDTA). Cells were surface-stained for 25 minutes at 4°C. For intracellular staining, cells were fixed and permeabilized using the eBioscience Foxp3 Fix/Perm buffer kit. For detection of IFNγ and TNFα, cells were stimulated with Cell Stimulation Cocktail for 5 hours. After 1 hour, GolgiStop was added to the cells. FACS analyses were performed using a Symphony flow cytometer (BD Biosciences). Data were analyzed using FlowJo software (Tree Star Inc.).

Antibodies

For animal studies murine IgG1 aPDL1 (clone 6E11), murine IgG1 anti-gp120 isotype control, rat IgG2a aCD40 (clone FGK45), and murine IgG1 anti-CSF1R (clone 2G2) antibodies were used. Antibodies were stored in 20 mmol/L histidine acetate, 240 mmol/L sucrose, and 0.02% polysorbate 20, pH 5.5 and diluted in PBS prior to use. Antibodies used for flow cytometry are listed in the Supplementary Methods.

Sublethal irradiation and mixed bone marrow chimeras

Recipient CD45.1 C57BL/6 mice (The Jackson Laboratory, stock no. 002014) were sublethally irradiated with 450 rads by using a Cesium 137 source. One day after irradiation, donor CD45.2 or IFNγR-deficient mice (The Jackson Laboratory, stock no. 003288) were euthanized and bone marrow was collected from femurs and tibias. Irradiated recipient mice were injected via tail vein with donor 2×10^6 bone marrow cells in 100 μL in sterile PBS/mouse. Tumor inoculation and tissue processing were performed as described previously.

Preparation of dissociated tumor supernatant

MC38 tumors were digested as described previously. Tumor homogenates were filtered through a 70-μm nylon filter (Corning) and centrifuged twice at 2,000 rpm for 5 minutes at 4°C. To remove treatment antibodies, tumor supernatants were incubated with Toyopearl (Tosoh Bioscience) for 5 minutes at room temperature (1:10 dilution) and centrifuged. Supernatants were then filtered through a 0.22-μm Vacuum Filter Unit (Corning, catalog no. 431153) on ice, aliquoted into tubes, and stored at −80°C before use.

OT-II purification and CFSE labeling

Spleens and lymph nodes from OT-II mice (The Jackson Laboratory, stock no. 004194) were harvested. Naïve OT-II cells were purified with Naive $CD4^+$ T Cell Isolation Kit (Miltenyi Biotec, catalog. no. 130-104-453). Cells were counted and labeled with CFSE using CellTrace CFSE Cell Proliferation Kit (Thermo Fisher Scientific, C34554) as described in the Supplementary Methods.

Bone marrow–derived macrophage polarization and OT-II coculture assay

Bone marrow–derived macrophage (BMDM) differentiation is described in the Supplementary Methods. On day 7 of differentiation, BMDMs were replenished with DMEM + 10% FBS + Penicillin/Streptomycin/GlutaMAX without M-CSF. Dissociated tumor supernatant media was added for macrophage polarization. When indicated, recombinant mouse IFNγ (PeproTech, 10ng/mL) or anti-mouse IFNγ rat IgG1 (BioXCell, clone: XMG1.2, 20 μg/mL) was added to the medium. On day 9, BMDMs were gently harvested, washed with PBS, plated in 96-well plates at 0.2×10^6 cells/well, and loaded with $OVA_{323\text{-}339}$ (AnaSpec) at 10 μg/mL for 3 hours at 37°C. After 3 extensive washes, CFSE-labeled naïve OT-II cells were added to the BMDM culture at 0.2×10^6 cells/well for 4 days before harvesting for FACS analysis.

Statistical analysis

All data were presented as means ± SD. Comparisons between tumor models, time points, or treatments were generated using nonparametric, Mann–Whitney tests, whereas cell subset comparisons within a given group were performed using paired *t* tests. For correlations, two-tailed nonparametric Spearman correlation analysis was used. Prism 6.0 (GraphPad) was used to process all the statistical analyses. Uncorrected *P* values were presented to validate RNA sequencing data.

RNA sequencing for transcriptome analysis

MC38 tumors of similar size between isotype and aPDL1-treated groups were collected, digested, and cell lysates stained (see Methods above). Macrophages and monocytes were sorted using a BD FACSAria. RNA was extracted and quantified with RNA Plus Mini Kit (Qiagen) according to the manufacturer's protocol. Concentration of RNA samples was determined using NanoDrop 8000 (Thermo Fisher Scientific) and integrity of RNA was determined by Fragment Analyzer (Advanced Analytical Technologies). tRNA (0.1 μg) was used as an input material for library preparation using TruSeq Stranded Total RNA Library Prep Kit (Illumina). Library establishment is described in the Supplementary Methods.

Differential gene expression and gene set enrichment analysis

After normalization using R/Bioconductor package DESeq2 (38), differential gene expression between cell types isolated from control-treated versus aPDL1-treated tumors was performed using R/Bioconductor package limma (39). Gene set enrichment analysis (GSEA) was performed for MSigDB collections c2, c5, and c7 (40) using camera (41) as implemented in the multiGSEA R package (http://github.com/lianos/multiGSEA). Enriched gene sets were filtered for those passing an FDR cutoff of 0.01 and a gene set size of $n < 150$. For visualization, only the 10 most up- and 10 most downregulated gene ontology (GO) sets are shown. These were manually grouped into broad functional categories

based on the genes that contributed most to the enrichment. A complete list of enriched gene sets is provided as Supplementary Table S1. Calculation of gene set scores and differential expression analysis for select genes and gene sets is described in the Supplementary Methods. (GEO accession number: GSE125383).

Results

Tumor macrophages have a suppressive phenotype that correlates with tumor burden

To investigate the effects of aPDL1 treatment on TAMs, we first focused on the baseline characteristics of the myeloid compartment in the MC38 tumor model given its partial responsiveness to treatment and its significant macrophage infiltration. $Ly6C^{-}Ly6G^{-}F4/80^{+}$ TAMs and $Ly6C^{+}$ inflammatory monocytes were present at high densities in tumors (52% and 22%, respectively) as the major tumor immune infiltrate (Supplementary Fig. S1A). TAMs in MC38 tumors expressed high levels of ARG1 and low but detectable levels of iNOS, whereas monocytes highly expressed iNOS and low levels of ARG1 (Supplementary Fig. S1B). $Ly6C^{int}$ cells expressed moderate levels of both ARG1 and iNOS, suggesting a transitional state (Supplementary Fig. S1B; refs. 2, 17). The majority of TAMs expressed high levels of both MHCII and CD206 and were identified as an M1/M2 intermediate subset. $MHCII^{+}CD206^{-}$ and $MHCII^{-}CD206^{+}$ TAMs were described as M1-like and M2-like, respectively (Fig. 1A, left). Further analysis showed that the M2-like and M1/M2 intermediate subsets had high ARG1 expression, whereas M1-like and M1/M2 intermediate subsets had high iNOS levels (Fig. 1A, right). This indicated that the M1/M2 intermediate subset displayed both immunosuppressive and proinflammatory phenotypes. Noteworthy, MHCII and iNOS levels on TAMs, as well as the M1-like frequency, were negatively associated with tumor burden (Fig. 1B). In contrast, CD206, ARG1 expression, and M2-like frequency were positively correlated with tumor size (Fig. 1C). Dynamically, the composition of TAMs shifted to a more suppressive M2-like phenotype as tumors progressed and tumor burden increased (Fig. 1D and E) consistent with previous reports (1, 4, 6).

aPDL1 treatment drives TAM polarization toward a more proinflammatory phenotype along with increased CD8 T-cell abundance and activity

Following aPDL1 treatment, MC38 tumor growth was significantly delayed with 10% complete responses (CR) in treated mice (Fig. 2A). We then examined the expression of various functional markers on TAMs 7 days after treatment initiation and at a time point both were treated and control tumors were still of comparable size (Supplementary Fig. S1C). aPDL1 treatment reduced ARG1 levels (Fig. 2B Supplementary Fig. S1C) mainly on ARG1-high–expressing M1/M2 intermediate and M2-like subsets (Fig. 2B). Conversely, iNOS, MHCII, and CD40 levels on TAMs, as well as iNOS levels on monocytes, increased following treatment (Fig. 2C and D; Supplementary Fig. S1C). CD8 T-cell infiltration, granzyme-B (GZMB) production, and the CD8/Treg ratio were also significantly elevated by treatment, consistent with previous reports of aPDL1-induced reinvigoration of CD8 T cells (Fig. 2E; refs. 31, 36). Interestingly, ARG1 levels on TAMs were negatively associated with the density, activation, and proliferation of CD8 T cells, whereas iNOS expression on TAMs was positively associated with the abundance and function of CD8 and CD4 T cells (Fig. 2F–G; Supplementary Fig. S1D and S1E), indicating a connection between T-cell activation and TAM polarization in tumors.

We next evaluated whether macrophage remodeling following aPDL1 treatment was contributed in part by newly differentiated macrophages from monocyte precursors. Monocytes were adoptively transferred into mice with established MC38 tumors treated with aPDL1 or isotype control antibodies. A similar level of monocyte recruitment and TAM differentiation was observed in the tumors after 2 days (Supplementary Fig. S1F). However, recently differentiated TAMs in aPDL1-treated mice were enriched in M1-like macrophages when compared with differentiated TAMs in isotype-treated mice (Fig. 2H) with lower levels of ARG1 and higher levels of iNOS and CD40 expression (Fig. 2I). In addition, recently recruited monocytes also displayed a more proinflammatory phenotype with elevated iNOS and CD40 expression in aPDL1-treated recipient tumors (Fig. 2J). Importantly, this induction of newly differentiated M1-like macrophages in aPDL1-treated mice coincided with a higher level of CTL infiltration, GZMB production, and a significant increase in the CD8/Treg ratio (Supplementary Fig. S1G), suggesting that the phenotypic changes imparted on newly differentiated TAMs provided a beneficial effect on the T-cell compartment. Together, these results corroborate that aPDL1 treatment induces a rapid and substantial change in the tumor microenvironment, which leads to a proinflammatory phenotype on monocytes and differentiating TAMs. Thus, the phenotypic changes observed in TAMs following aPDL1 treatment are in part contributed by newly differentiated monocyte-derived macrophages that are imprinted with a more proinflammatory phenotype.

aPDL1 treatment leads to genome-wide TAM polarization toward a more proinflammatory phenotype

To expand our understanding and complement the phenotypic analysis of TAMs using cell surface markers, we performed whole-transcriptome profiling of macrophages sorted from aPDL1 and control-treated tumors. GSEA revealed profound genome-wide repolarization, evidenced by an elevated expression of the antigen presentation machinery including various gene sets made up of MHC molecules and phagocytosis/opsonization–related Fcγ receptors (Fig. 3A; complete lists of enriched gene sets in Supplementary Table S1). Furthermore, predefined gene sets for IFNγ downstream, proinflammatory signaling and chemokine expression, TLR/NFκB, and the autophagy pathway were also upregulated in macrophages following aPDL1 treatment (Fig. 3B; Supplementary Fig. S2A and S2B). Interestingly, GSEA uncovered a concomitant downregulation of numerous collagen-related gene sets, potentially reflecting tissue remodeling, as well as development-related gene sets in macrophages (Fig. 3A). aPDL1 treatment had a similar effect on intratumoral monocytes (Supplementary Fig. S2C and S2D), indicating a substantial and significant influence of PDL1 blockade on both macrophages and their precursors in agreement with a recent publication (37).

aPDL1–mediated remodeling of the macrophage compartment is IFNγ dependent

To identify the factor(s) linking aPDL1-induced T-cell reinvigoration and TAM polarization, we performed cytokine profile analysis of MC38 tumor lysates. We observed a marked upregulation of IFNγ following aPDL1 treatment (Fig. 4A), which was mainly produced by intratumoral CD8 T cells (Fig. 4B). IFNγ was

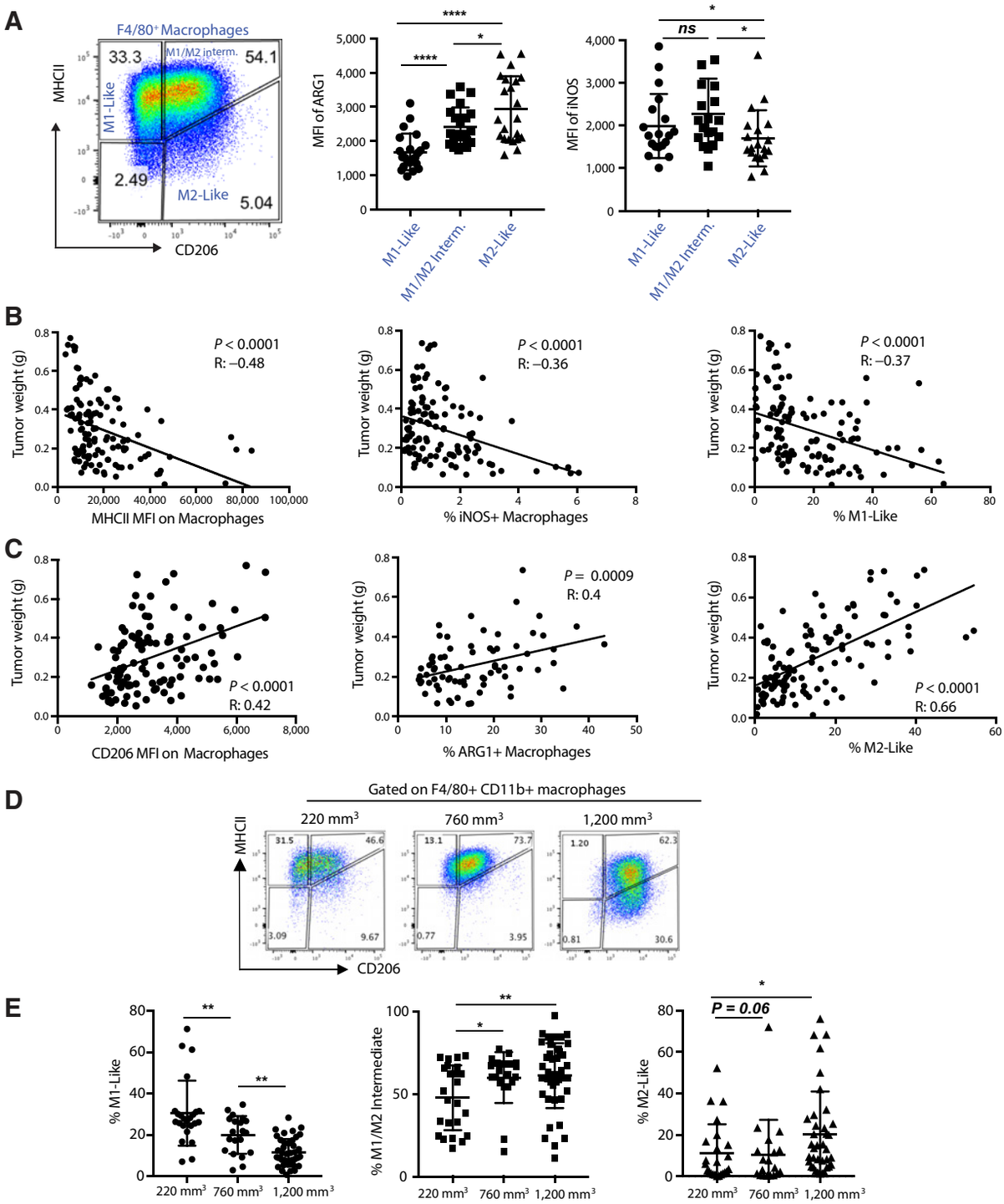

Figure 1.

Tumor macrophages have a suppressive phenotype that correlates with tumor burden. MC38 tumors were collected 1 day after they reached an average size of approximately 180 mm^3 and single-cell suspensions were prepared for flow cytometry analysis. Single-cell suspensions were stained and intratumoral macrophages were defined as $CD45^+Dump^-CD11b^+CD11c^-F4/80^+$ cells. **A,** Left, representative FACS plot showing M1-like, M1/M2 intermediate, and M2-like subsets based on MHCII and CD206 staining. Right, mean fluorescent intensity (MFI) of ARG1 and iNOS on macrophage subsets. **B,** Correlation between M1 markers (MHCII and iNOS) and M1-like frequency and tumor weight. **C,** Correlation between M2 markers (CD206 and ARG1) and M2-like frequency and tumor weight. **D,** Representative FACS plots of M1/M2 subsets based on CD206/MHCII staining on macrophages from tumors of different sizes. **E,** Comparison of M1-like (left), M1/M2-intermediate (middle), or M2-like frequencies (right) from **D**. $N = 20$ (220 mm^3 and 760 mm^3) and 40 (120 mm^3), respectively. *, $P < 0.05$; **, $P < 0.01$; ****, $P < 0.0001$. ns, nonsignificant.

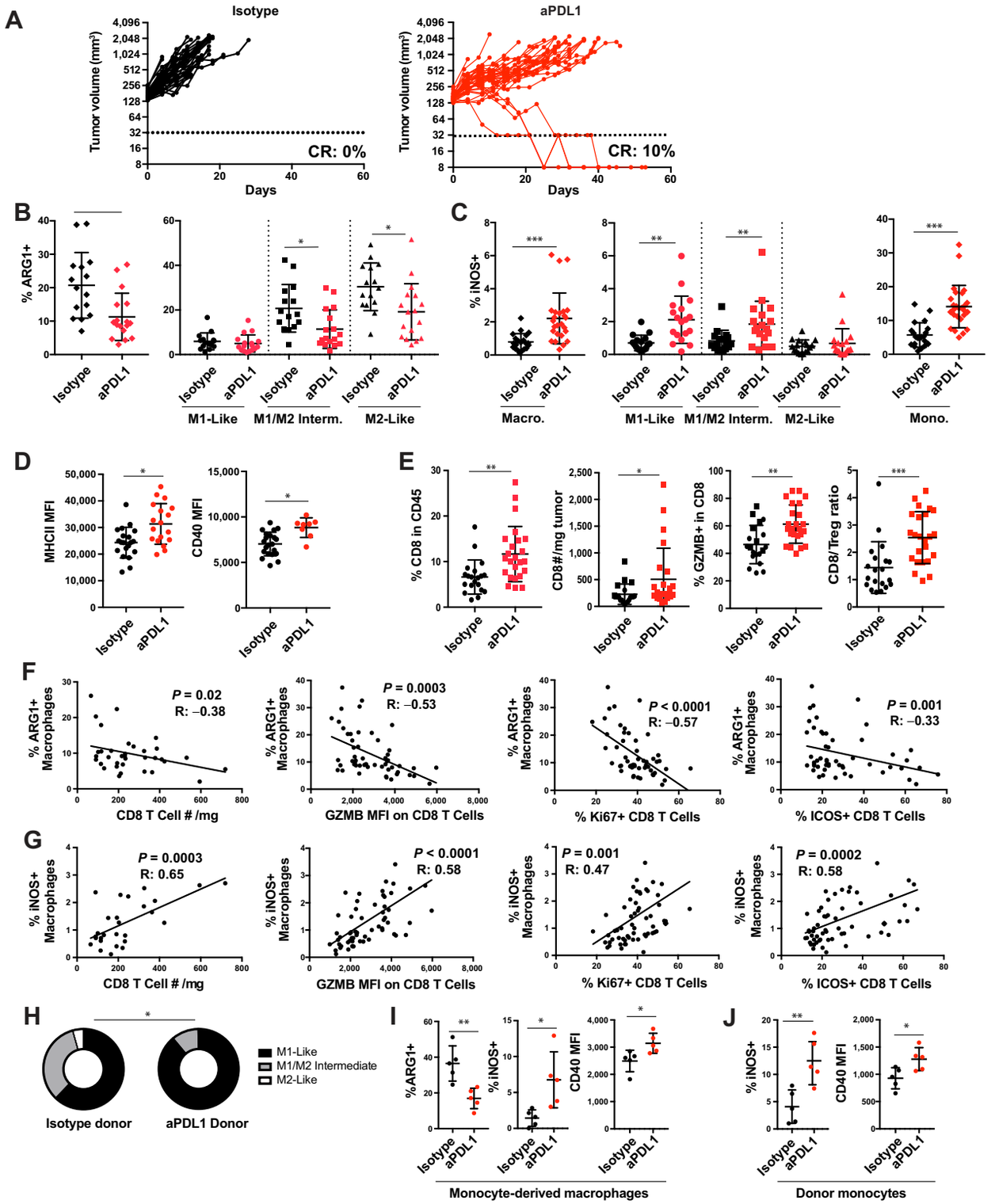

Figure 2.

aPDL1 treatment drives TAM polarization toward a more proinflammatory phenotype along with increased CD8 T-cell numbers. Mice were inoculated with MC38 tumor cells and once tumors reached a volume of approximately 180 mm^3 (day 0), mice with similarly sized tumors were grouped into treatment arms. The next day (day 1), mice were dosed with aPDL1 or isotype control antibody at 10 mg/kg i.v. for the first dose and 5 mg/kg i.p., thereafter twice a week for 3 weeks. Tumors were also collected 7 days after treatment initiation, digested, and single-cell suspensions used for FACS analysis. **A,** Tumor volume (mm^3) of control (black) or aPDL1 (red)-treated mice is shown on a $\log_2$ scale; $N = 10$. (*Continued on the following page.*)

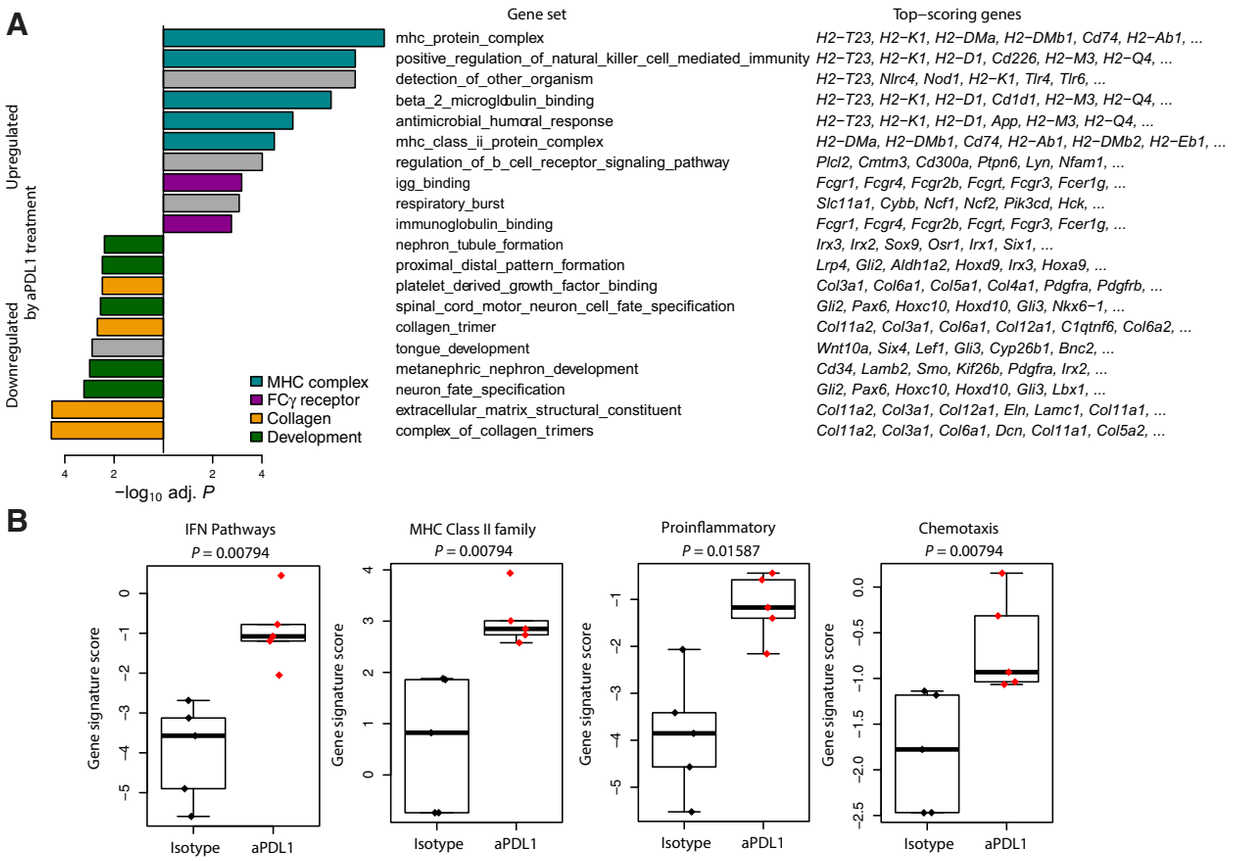

Figure 3.

aPDL1 treatment leads to genome-wide TAM polarization toward a more proinflammatory phenotype. TAMs were sorted from untreated or aPDL1-treated MC38 tumors 7 days after treatment. RNA was subsequently purified for high-throughput sequencing. **A,** Select GO gene sets enriched in genes differentially expressed in macrophages isolated from control versus aPDL1-treated tumors. Shown are adjusted $-\log_{10} P$ values for enrichment of the ten most significantly up- and significantly downregulated GO gene sets in aPDL1-treated macrophages. Gene sets that are inferred to reflect key underlying biological processes are colored. Only the top six genes per set (ranked by single-gene P value) are shown. **B,** Expression of predefined gene sets (see Supplementary Table S1) representing pathways of interest in isotype versus aPDL1-treated macrophages. Expression of all genes within a set was summarized into one score. Differential expression of gene set scores was assessed using two-sided Wilcoxon rank-sum tests. $N = 5$/group.

critical for aPDL1-mediated efficacy, as IFNγ blockade abolished aPDL1-mediated antitumor responses and the abundance of IFNγ was negatively correlated with tumor weight and the frequency of M2-like cells (Supplementary Fig. S3A–S3C). We therefore examined TAM polarization during aPDL1 treatment with blockade of IFNγ, a known driver of M1 differentiation (4, 8, 42), and observed abrogation of M1-like skewing with an increased frequency of suppressive M2-like macrophages (Fig. 4C). Moreover, IFNγ blockade abated the propolarization changes in ARG1, iNOS, and MHCII expression following aPDL1 treatment and reduced the overall levels of CD40 expression (Fig. 4D).

We next investigated the capacity of the macrophage compartment to respond to changes in environmental IFNγ by transferring IFNγR$^{-/-}$ bone marrow into sublethally irradiated wild-type animals. Following reconstitution, TAMs consisted of a mixed population of either IFNγR positive (IFNγR$^{+/+}$) or negative

(*Continued.*) **B,** Frequency of arginase-expressing cells (ARG1^{+}) in total macrophages and macrophage subsets following treatment. **C,** Frequency of iNOS-expressing cells in total macrophages, macrophage subsets, and monocytes. **D,** Expression levels (mean fluorescent intensity, MFI) of MHCII and CD40 on macrophages following treatment. **E,** Frequency and absolute number of intratumoral CD8 T cells, frequency of GZMB-producing cells, and the CD8/Treg ratio. **F,** Correlation between the frequency of ARG1^{+} macrophages and CD8 T-cell abundance or GZMB, Ki67, and ICOS levels. **G,** Correlation between the frequency of iNOS^{+} macrophages and CD8 T-cell abundance or GZMB, Ki67, and ICOS levels. $N = 26$. **H,** CD45.1 monocytes (donor) were adoptively transferred into CD45.2 MC38 tumor–bearing animals (recipient) treated with isotype or aPDL1 antibodies. Two days after transfer, tumors were harvested and stained for FACS analysis. **H,** Pie charts depicting the proportion of M1/M2 subsets in recently differentiated donor-derived TAMs. **I,** Frequency of ARG1^{+} and iNOS^{+} cells as well as CD40 MFI on donor-derived TAMs. **J,** Frequency of iNOS^{+} cells and CD40 MFI on donor-derived monocytes. $N = 5$; *, $P < 0.05$; **, $P < 0.01$; ***, $P < 0.001$.

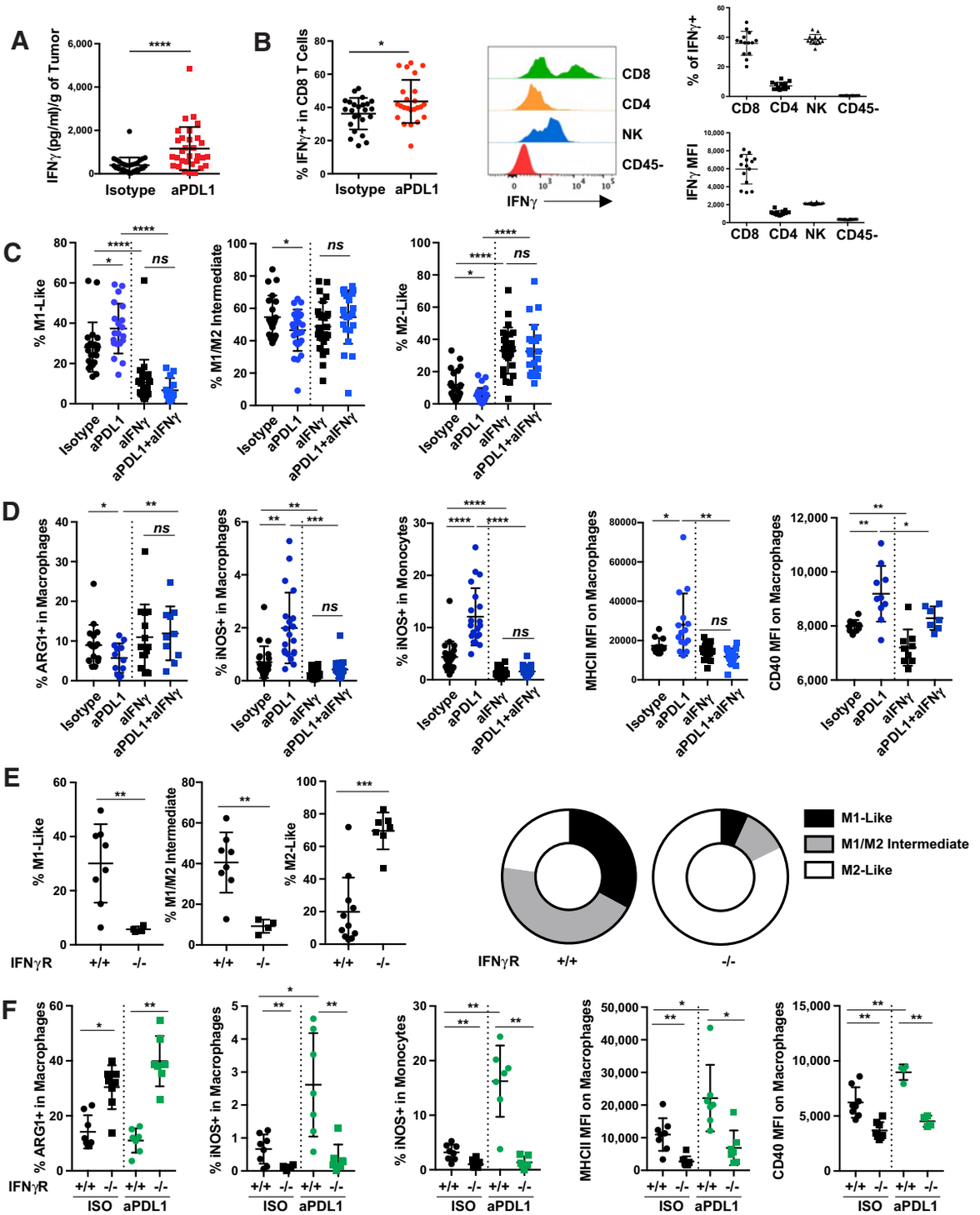

Figure 4.

aPDL1 remodeling of the macrophage compartment is IFNγ-mediated and dependent on IFNγR expression on TAMs. **A,** IFNγ levels as measured by Luminex from MC38 tumor supernatant from isotype or aPDL1-treated tumors. **B,** Frequency of IFNγ$^+$ cells among intratumoral CD8 T cells and IFNγ-expressing cell subsets and mean fluorescent intensity (MFI) following treatment. **C** and **D,** MC38 tumors were treated with isotype or aPDL1 antibodies in the presence or absence of neutralizing anti-IFNγ. **C,** Frequency of M1/M2 subsets following treatment. **D,** Frequency of ARG1$^+$ and iNOS$^+$ macrophages (or monocytes), as well as MHCII expression on macrophages. **E,** WT and IFNγR-deficient mixed bone marrow chimeras were inoculated with MC38 and once tumors became established, mice were randomized and treated with aPDL1 or isotype control antibody. Frequency of M1/M2 subsets among WT (+/+) and IFNγR-deficient (−/−) macrophages. **F,** Frequency of ARG1$^+$ and iNOS$^+$ macrophages as well as MHCII and CD40 levels. *, $P < 0.05$; **, $P < 0.01$; ***, $P < 0.001$; ****, $P < 0.0001$; ns, nonsignificant.

($IFN\gamma R^{-/-}$) cells. We observed a pronounced shift to a suppressive M2-like phenotype in $IFN\gamma R^{-/-}$ TAMs at baseline (Fig. 4E). ARG1 levels were also increased while iNOS, MHCII, and CD40 expression was significantly decreased in $IFN\gamma R^{-/-}$ macrophages compared with their $IFN\gamma R^{+/+}$ counterparts, which persisted even after aPDL1 treatment (Fig. 4F). These results corroborate the major role of intratumoral IFNγ levels in mediating the phenotypic skewing of the macrophage compartment in tumors. Collectively, these findings demonstrate a direct cross-talk between IFNγ, mainly produced by CD8 T cells following aPDL1 treatment, and remodeling of the macrophage compartment.

Dissociated tumor supernatant from aPDL1-treated tumors drives BMDM polarization that enhances T-cell proliferation and activation

To further interrogate the relationship between the tumor microenvironment following aPDL1 treatment and the polarization of TAMs, we developed a BMDM polarization assay using dissociated tumor supernatant from *ex vivo*–digested MC38 tumors. Dissociated tumor supernatant from untreated tumors led to robust M2-like polarization, with its effect gradually weakening with serial dilution (Supplementary Fig. S4A). Exogenous IFNγ robustly polarized BMDMs in the presence of dissociated tumor supernatant, reducing ARG1 levels and increasing iNOS, MHCII, and CD40 expression (Supplementary Fig. S4B and S4C). Importantly, dissociated tumor supernatant from aPDL1-treated tumors, moderately but significantly polarized macrophages from M2-like to an intermediate state and elevated their expression of MHCII and CD40, as well as MHCI, CD86, and FcγRI (Fig. 5A), consistent with the gene expression profiling in sorted macrophages from aPDL1-treated tumors *in vivo* (Fig. 3; Supplementary Fig. S2B). In addition, dissociated aPDL1-treated tumor supernatant decreased ARG1 levels while increasing iNOS expression (Supplementary Fig. S4D), albeit the frequency of iNOS-producing BMDMs was low. Importantly, combining dissociated tumor supernatant from aPDL1-treated tumors with IFNγ blockade reverted most of the phenotypic changes observed, suggesting that IFNγ is a major driver of BMDM polarization in dissociated tumor supernatants from aPDL1-treated tumors.

We next examined the functional output of polarized BMDMs by coculture of $OVA_{323\text{-}339}$–loaded BMDMs with CFSE-labeled OT-II cells. BMDMs polarized with dissociated tumor supernatant from aPDL1-treated tumors, or tumor supernatant supplemented with exogenous IFNγ, induced robust OT-II proliferation as determined by CFSE dilution (Fig. 5B; Supplementary Fig. S4E and S4F). In addition, these OT-II cells significantly upregulated their expression of the activation markers CD69 and CD25 and showed increased coexpression of CD44 and ICOS when compared with OT-II cells cocultured with control polarized BMDMs (Fig. 5B; Supplementary Fig. S4F). Furthermore, blockade of IFNγ during the course of BMDM polarization with dissociated tumor supernatant from aPDL1-treated tumors, partially abrogated the subsequent proliferation and activation of OT-II cells (Fig. 5B). These results illustrate that increased IFNγ levels following aPDL1 treatment can impact not only the phenotype of TAMs, but more importantly, enhance their ability to promote T-cell activation and proliferation. Tumor macrophages therefore represent an indirect downstream target of aPDL1 treatment in responsive tumors, which can form a positive feedback loop to T cells.

Remodeling of the macrophage compartment is observed in aPDL1-responsive tumor models

To expand our understanding of aPDL1-mediated macrophage remodeling, we studied two additional tumor models: EMT6 that also responds to aPDL1, and JC that is refractory to treatment. These two tumor models have substantial TAM infiltration but exhibit different overall immune profiles and TAM phenotypes (Supplementary Fig. S5A and S5B). Following aPDL1 treatment, there was a shift from M2-like to M1-like macrophages in EMT6, but not in JC tumors (Supplementary Fig. S5C). Furthermore, there was a significant decrease in the absolute numbers of ARG1-producing macrophages and an increase in the frequency of iNOS-producing TAMs and monocytes, as well as their MHCII and CD40 expression in EMT6 similar to MC38, but this was not observed in JC tumors (Supplementary Fig. S6A–S6D). These observations indicate a possible and consistent remodeling of the macrophage compartment in aPDL1-responsive tumor models that is absent in a nonresponsive tumor context. This was likely due, in part, to a lack of IFNγ induction following aPDL1 treatment in JC tumors (Supplementary Fig. S6E and S6F) and a more suppressive TAM phenotype given the lower IFNγ levels at baseline in JC when compared with MC38 and EMT6 tumors.

TAM phenotype and density influences the level of macrophage remodeling

Given the direct polarizing effect of agonistic aCD40 on TAMs (8, 22, 27), we investigated the capacity of aCD40 to further push the remodeling mediated by aPDL1 in different tumor immune contextures. To that end, we used macrophage-rich MC38 and EMT6 tumors (Supplementary Fig. S1A and S5A), with MC38 having a higher baseline abundance of macrophages with increased ARG1 expression and decreased iNOS levels when compared with macrophages in EMT6 tumors (Fig. 6A). Both models respond to aPDL1 treatment, but antitumor activity (Fig. 6B) and the remodeling effect of aPDL1 on TAMs were more pronounced in EMT6 than MC38 tumors (Fig. 2A–C; Supplementary Fig. S6A–S6C). This led us to speculate that further polarizing macrophages with aCD40 would combine more effectively with aPDL1 in the EMT6 tumor model given its lower macrophage burden and less suppressive phenotype. Indeed, as soon as 48 hours after a single dose of aCD40, a significant remodeling of the macrophage compartment was observed in EMT6, characterized by potentiated M1-like polarization and a marked increase in MHCII and MHCI expression with decreased CD206 and ARG1 (Fig. 6C). Some combinatorial effects with aPDL1 were already noticeable (i.e., CD206 and ARG1), but iNOS levels were not substantially changed at this time point. On the other hand, aCD40 led to milder M1-like polarization on macrophages in MC38, mainly associated with a reduction in CD206 (Fig. 6D). There were no combinatorial effects with aPDL1 based on the markers examined. These results suggest that reinforcing the polarization of macrophages by combining aPDL1 with aCD40 can further unleash antitumor activity, but the combinatorial effect is likely dependent on various parameters including the abundance and baseline phenotype of TAMs.

Combining aCD40 with aCSF1R has recently been shown to augment responses when compared with either treatment alone (27) and a single dose of aCSF1R was sufficient to significantly reduce both macrophage and monocyte numbers in tumors, without affecting CD8 T-cell abundance (Fig. 7A). We thus speculated that in the MC38 tumor model, in which

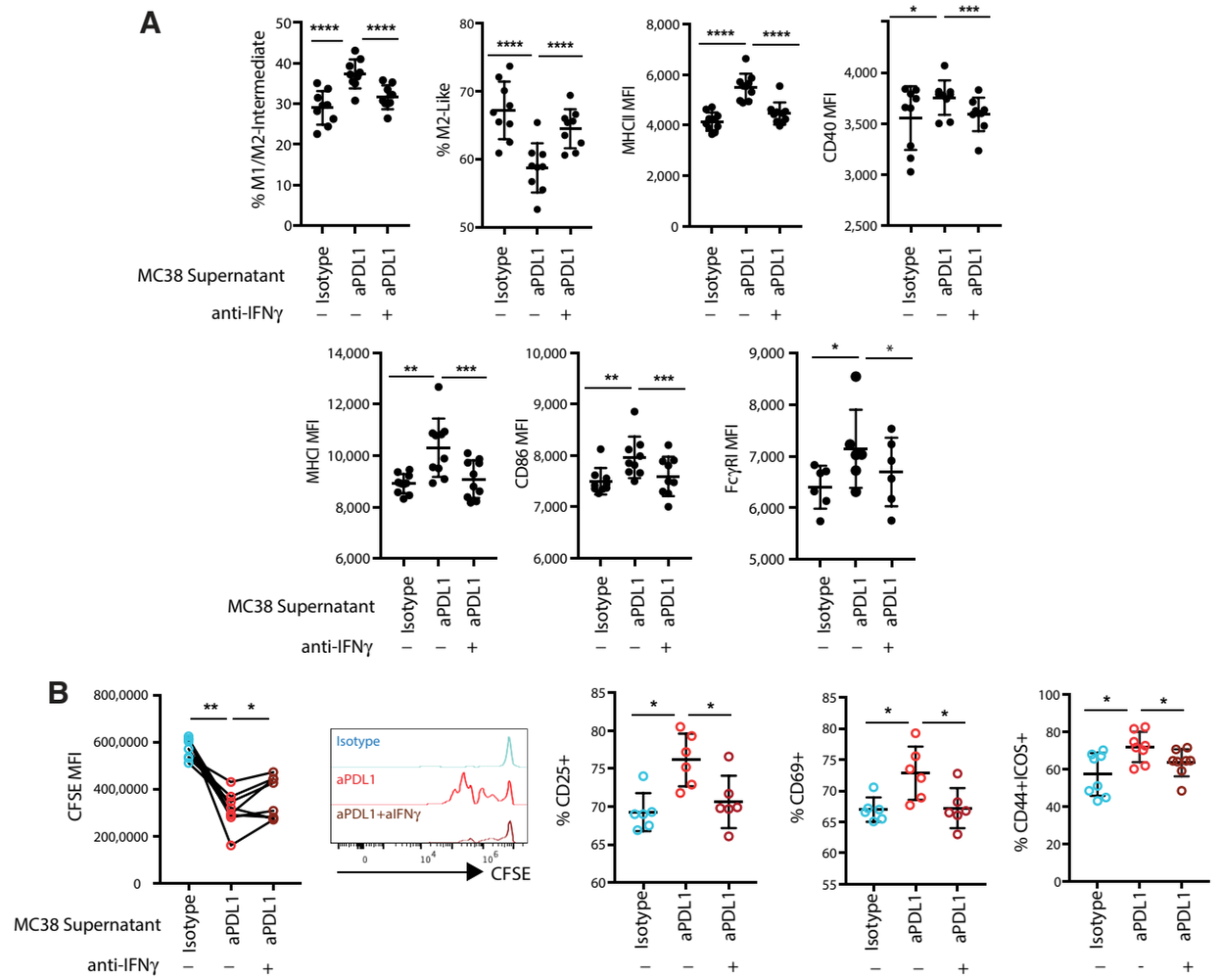

Figure 5.

Dissociated tumor supernatant from aPDL1-treated tumors drives BMDM polarization that enhances T-cell proliferation and activation. MC38 tumors from isotype or aPDL1-treated mice were digested and supernatant collected for subsequent assays. BMDMs were generated and polarized with tumor supernatant in the presence or absence of a neutralizing aIFNγ antibody. **A,** Frequency of M1/M2 subsets and MHCII, CD40, MHCI, CD86, and FcγRI (CD64) expression levels on BMDMs polarized with supernatant from isotype or aPDL1-treated tumors. **B,** BMDMs were loaded with $OVA_{323-339}$ and cocultured with CFSE-labeled naïve OT-II cells. OT-II cell proliferation and activation were determined by CFSE dilution, CD25, and CD69 staining, as well as CD44 and ICOS coexpression, respectively. Lines connect data acquired from the same bone marrow donor. Paired *t* tests were performed. *, $P < 0.05$; **, $P < 0.01$; ***, $P < 0.001$; ****, $P < 0.0001$. MFI, mean fluorescent intensity.

combination of aPDL1 with aCD40 was insufficient to significantly remodel the macrophage compartment, reducing the suppressive macrophage burden by polarizing and depleting TAMs would maximize the antitumor activity mediated by aPDL1. Like aCD40, aCSF1R only mildly synergized with aPDL1 treatment, implying the limited benefit of either macrophage polarization or depletion in MC38 (Fig. 7B and C). Combination of aCD40 with aCSF1R, however, elicited a robust antitumor response, resulting in 70% CRs and corroborating the immune-suppressive characteristic of TAMs in this tumor model. Remarkably, the combination of aCD40 and aCSF1R with aPDL1 demonstrated the strongest combinatorial activity, resulting in 90% CRs and clearly improving the efficacy of aPDL1 or any other two-agent combinations. These results suggest that in tumor immune contextures that are characterized by a high density of suppressive TAMs, remodeling of the macrophage compartment by aPDL1 or even a more direct polarizing agent like aCD40 might not be enough to enhance responses. Here, both macrophage depletion and polarization will likely be needed to efficiently reduce macrophage burden and further unleash aPDL1-mediated T-cell responses.

Discussion

TAMs are shaped by the tumor microenvironment and they, in turn, actively shape their microenvironment. Tumor macrophages can have diverse cross-talk with other immune cell subsets, and their phenotype and function can vary among tumor types and stages of disease. In this study, we show that aPDL1 treatment can remodel the macrophage compartment, resulting in a more proinflammatory phenotype in both monocytes and

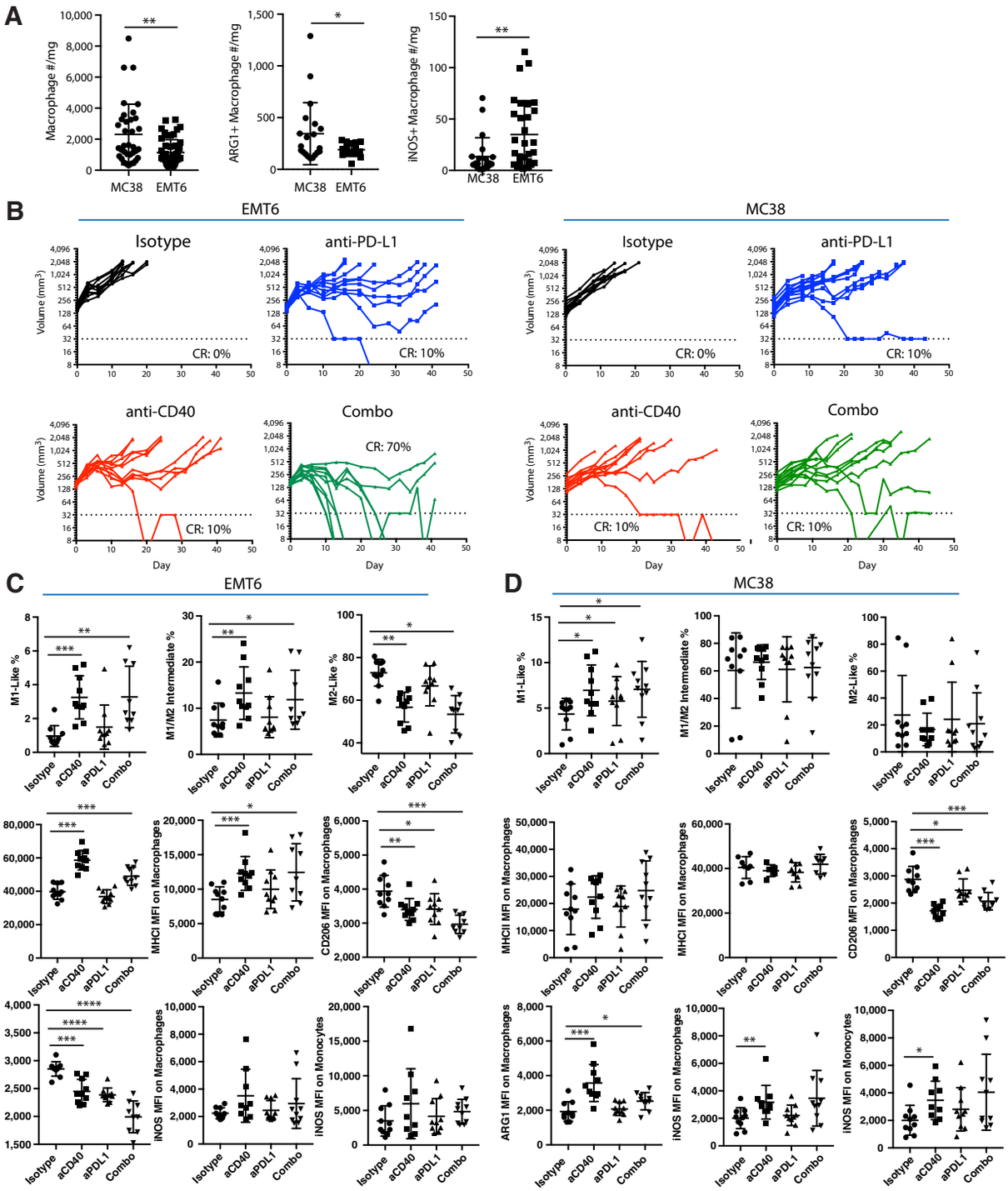

Figure 6.

Directed TAM polarization with aCD40 combines effectively with aPDL1 in the EMT6 tumor model. Mice were inoculated with either MC38 or EMT6 tumor cells and once tumors reached a volume of approximately 180 mm^3 (day 0), mice with similarly sized tumors were randomized into treatment groups. The next day (day 1), mice were dosed with either isotype control (anti-gp120), aPDL1, or a single dose of aCD40. **A,** Absolute number of total, $ARG1^+$, and $iNOS^+$ macrophages per mg of tissue in MC38 and EMT6 tumors at baseline. **B,** Tumor volume (mm^3) of control (black), aPDL1 (blue), aCD40 (red), or combo (green)-treated EMT6 and MC38 tumor–bearing mice is shown on a $\log_2$ scale; $N = 10$/group. **C** and **D,** Pharmacodynamic analysis of tumor macrophages 48 hours after treatment initiation evaluating the M1/M2-like subset frequency and the expression of MHCI, MHCII, CD206, ARG1, and iNOS. *, $P < 0.05$; **, $P < 0.01$; ***, $P < 0.001$; ****, $P < 0.0001$. MFI, mean fluorescent intensity.

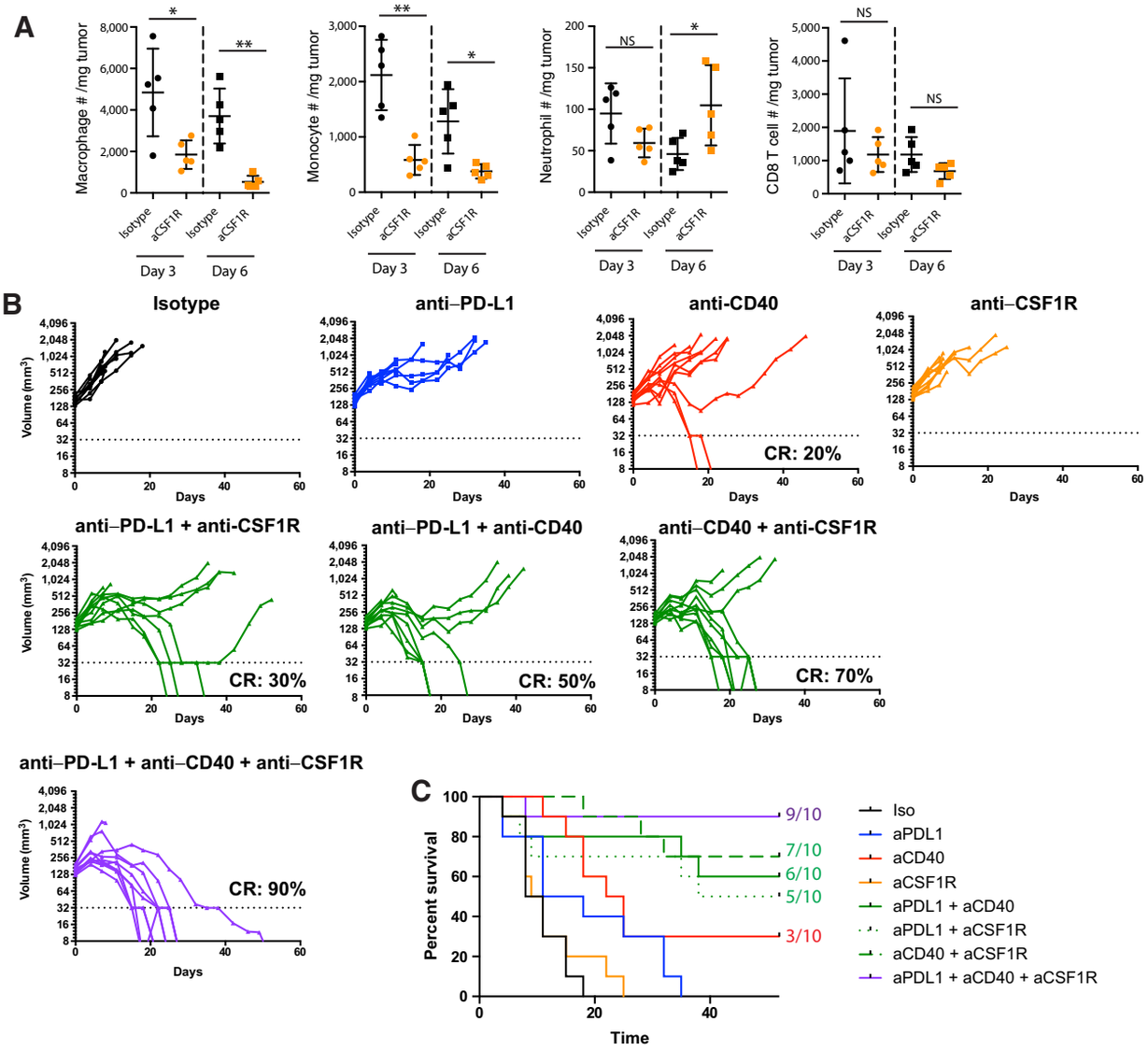

Figure 7.

TAM polarization and depletion combine effectively with aPDL1 treatment in the MC38 tumor model. Mice were inoculated with MC38 and once tumors reached a volume of approximately 180 mm^3 (day 0), mice with similarly sized tumors were randomized into treatment groups. The next day (day 1), mice were dosed with either isotype control, aPDL1, aCD40 (4 mg/kg single dose), or aCSF1R (30 mg/kg single dose) alone or in combination. **A,** Abundance of intratumoral immune infiltrates 3 and 6 days after a single dose of aCSF1R. **B,** Tumor volume (mm^3) of control (black), aPDL1 (blue), aCD40 (red), aCSF1R (orange), combination of two (green), or three agents (purple)-treated MC38 tumor–bearing mice is shown on a $\log_2$ scale. **C,** Survival curves from treatment groups in **B**. $N = 10$ mice per group. *, $P < 0.05$; **, $P < 0.01$; NS, nonsignificant.

macrophages. This was evidenced not only by changes in canonical M1/M2 marker expression like ARG1, iNOS, MHCII, and CD40, but also by increased expression of genes associated with antigen uptake, processing and presentation machinery, proinflammatory cytokines and T-cell–recruiting chemokines. We further demonstrate that TAM polarization was largely mediated by increased IFNγ signaling and required IFNγR expression on TAMs. We also find that while remodeling of the macrophage compartment was observed in responsive MC38 and EMT6 tumors, this was not evident in nonresponsive JC, which had lower IFNγ induction following treatment. Our results are in agreement with recent findings by Gubin and colleagues who observed a similar polarization and remodeling of the macrophage compartment largely mediated by IFNγ following aPD1 and aCTLA4 treatment and that initiated at the monocytic precursor stage (37). Together, our results confirm that the phenotype of the intratumoral macrophage compartment is influenced by the cytokine milieu that can be altered by treatment and provides new insights into the mechanism of action of checkpoint inhibitors.

Importantly, we demonstrate that aPDL1-mediated macrophage polarization had a beneficial effect on T-cell responses increasing their proliferation and cytolytic potential.

Functionally, BMDMs polarized with dissociated tumor supernatant from aPDL1-treated tumors were significantly more effective at driving the proliferation and activation of OVA-specific T cells *in vitro* than control-treated BMDMs, suggesting a beneficial, functional consequence of macrophage polarization induced by aPDL1-mediated microenvironment changes. This was further evidenced by transfer of monocytes into aPDL1-treated tumors that led to the differentiation of TAMs toward a more proinflammatory phenotype as well as an increase in CTL infiltration and GZMB expression. Polarization of macrophages following aPDL1 treatment can therefore improve T-cell responses. Our results highlight the beneficial impact of aPDL1 in shaping the macrophage compartment in responsive tumor models, which in turn can provide a positive feedback loop to T cells, thus supporting the notion for directly targeting these innate immune cells to further augment T-cell activity.

Agonistic aCD40 has been shown to rapidly activate macrophages and enhance their tumoricidal capacity alone or in combination with other TAM-targeting approaches (2, 22, 27, 28). In our studies, combining aPDL1 with a single dose of aCD40 led to an appreciable enhancement in antitumor activity demonstrating a further reduction in suppressive mechanisms that control antitumor responses when direct macrophage polarization was combined with aPDL1. However, although a single dose of aCD40 was sufficient to significantly augment responses in EMT6 tumors, the combinatorial effect with aPDL1 was milder in MC38. It is important to point out that the observed combinatorial activity with aCD40 could also be due to activation of dendritic cells, B cells, or other nonimmune cells–expressing CD40, but at least in the models tested, macrophages represent the major immune infiltrate and are likely playing a major role in the response to aCD40 (Supplementary Figs. S1A and S5A).

Given that a high density of TAMs could represent a larger suppressive barrier to overcome for antitumor activity, reducing the TAM compartment has recently been suggested (28) and is likely needed to enhance aPDL1 responses in tumor immune contextures highly infiltrated by macrophages. Indeed, we observed that combining aPDL1 with aCD40 and aCSF1R maximized antitumor activity in the macrophage-rich MC38 tumor model, whereas combining aPDL1 with either aCD40 or aCSF1R showed only a mild combinatorial response. Importantly, the combination of aCD40 with aCSF1R in the absence of aPDL1 significantly augmented responses, demonstrating the contribution of TAMs to inhibiting antitumor responses.

Together, our results demonstrate that aPDL1 can impart a phenotypic change on the macrophage compartment mainly through increased IFNγ levels and that this recently appreciated mechanism of action can be further augmented by direct macrophage targeting approaches. However, in the clinical setting, tumors characterized by a high level of suppressive TAMs could derive more benefit from aPDL1 treatment by combining macrophage polarization and depleting strategies. This approach could help proestablish a lower threshold for antitumor activity, potentially expanding the proportion and depth of responding individuals to checkpoint blockade.

Disclosure of Potential Conflicts of Interest

H. Xiong, S. Mittman, R. Rodriguez, M. Moskalenko, P. Pacheco-Sanchez, Y. Yang, D. Nickles, and R. Cubas have ownership interest (including stocks and patents) in Roche.

Authors' Contributions

Conception and design: H. Xiong, R. Cubas
Development of methodology: H. Xiong, S. Mittman, R. Rodriguez, R. Cubas
Acquisition of data (provided animals, acquired and managed patients, provided facilities, etc.): H. Xiong, S. Mittman, R. Rodriguez, M. Moskalenko, P. Pacheco-Sanchez, Y. Yang, R. Cubas
Analysis and interpretation of data (e.g., statistical analysis, biostatistics, computational analysis): H. Xiong, S. Mittman, M. Moskalenko, P. Pacheco-Sanchez, Y. Yang, D. Nickles, R. Cubas
Writing, review, and/or revision of the manuscript: H. Xiong, M. Moskalenko, P. Pacheco-Sanchez, Y. Yang, D. Nickles, R. Cubas
Administrative, technical, or material support (i.e., reporting or organizing data, constructing databases): S. Mittman, R. Rodriguez, M. Moskalenko, P. Pacheco-Sanchez, Y. Yang, D. Nickles, R. Cubas
Study supervision: R. Cubas

Acknowledgments

The authors would like to thank the core dosers and the cell line core group at Genentech for their contribution to this project as well as John Silva and Sharon Yee for their help with the anti-CSF1R study. They would also like to thank the flow cytometry core group for their help with cell sorting.

The costs of publication of this article were defrayed in part by the payment of page charges. This article must therefore be hereby marked *advertisement* in accordance with 18 U.S.C. Section 1734 solely to indicate this fact.

Received October 11, 2018; revised December 12, 2018; accepted January 17, 2019; published first January 24, 2019.

References

1. Noy R, Pollard JW. Tumor-associated macrophages: from mechanisms to therapy. Immunity 2014;41:49–61.
2. Mantovani A, Marchesi F, Malesci A, Laghi L, Allavena P. Tumour-associated macrophages as treatment targets in oncology. Nat Rev Clin Oncol 2017;14:399–416.
3. Chen D, Mellman I. Elements of cancer immunity and the cancer-immune set point. Nature 2017;541:321–30.
4. Biswas SK, Mantovani A. Macrophage plasticity and interaction with lymphocyte subsets: cancer as a paradigm. Nat Immunol 2010;11:889–96.
5. Mantovani A, Sica A, Sozzani S, Allavena P, Vecchi A, Locati M. The chemokine system in diverse forms of macrophage activation and polarization. Trends Immunol 2004;25:677–86.
6. Martinez FO, Gordon S. The M1 and M2 paradigm of macrophage activation: time for reassessment. F1000Prime Rep 2014;6:13.
7. Lawrence T, Natoli G. Transcriptional regulation of macrophage polarization: enabling diversity with identity. Nat Rev Immunol 2011;11:750–61.
8. Baer C, Squadrito M, Laoui D, Thompson D, Hansen S, Kiialainen A, et al. Suppression of microRNA activity amplifies IFN-γ-induced macrophage activation and promotes anti-tumour immunity. Nat Cell Biol 2016;18:790–802.
9. Thorsson V, Gibbs D, Brown S, Wolf D, Bortone D, Yang T-H, et al. The immune landscape of cancer. Immunity 2018;48:812—30.
10. Su S, Zhao J, Xing Y, Zhang X, Liu J, Ouyang Q, et al. Immune checkpoint inhibition overcomes ADCP-induced immunosuppression by macrophages. Cell 2018;175:442–457.
11. Bronte V, Zanovello P. Regulation of immune responses by L-arginine metabolism. Nat Rev Immunol 2005;5:nri1668.
12. Lechner M, Lirk P, Rieder J. Inducible nitric oxide synthase (iNOS) in tumor biology: the two sides of the same coin. Semin Cancer Biol 2005;15:277–89.
13. Burke AJ, Sullivan FJ, Giles FJ, Glynn SA. The yin and yang of nitric oxide in cancer progression. Carcinogenesis 2013;34:503–12.

14. Georgoudaki A-M, Prokopec KE, Boura VF, Hellqvist E, Sohn S, Östling J, et al. Reprogramming tumor-associated macrophages by antibody targeting inhibits cancer progression and metastasis. Cell Reports 2016;15: 2000–11.
15. Gao J, Ward J, Pettaway C, Shi L, Subudhi S, Vence L, et al. VISTA is an inhibitory immune checkpoint that is increased after ipilimumab therapy in patients with prostate cancer. Nat Med 2017;23:551–55.
16. De Henau O, Rausch M, Winkler D, Campesato LF, Liu C, Cymerman DH, et al. Overcoming resistance to checkpoint blockade therapy by targeting PI3Kγ in myeloid cells. Nature 2016;539:443–7.
17. Qian B-ZZ, Li J, Zhang H, Kitamura T, Zhang J, Campion LR, et al. CCL2 recruits inflammatory monocytes to facilitate breast-tumour metastasis. Nature 2011;475:222–5.
18. Franklin RA, Liao W, Sarkar A, Kim MV, Bivona MR, Liu K, et al. The cellular and molecular origin of tumor-associated macrophages. Science 2014;344: 921–5.
19. McCracken MN, Cha AC, Weissman IL. Molecular pathways: activating T cells after cancer cell phagocytosis from blockade of CD47 "Don't Eat Me" signals. Clin Cancer Res 2015;21:3597–601.
20. Tseng D, Volkmer J-PP, Willingham SB, Contreras-Trujillo H, Fathman JW, Fernhoff NB, et al. Anti-CD47 antibody-mediated phagocytosis of cancer by macrophages primes an effective antitumor T-cell response. Proc Natl Acad Sci U S A 2013;110:11103–8.
21. Zhu Y, Knolhoff BL, Meyer MA, Nywening TM, West BL, Luo J, et al. CSF1/CSF1R blockade reprograms tumor-infiltrating macrophages and improves response to T-cell checkpoint immunotherapy in pancreatic cancer models. Cancer Res 2014;74:5057–69.
22. Beatty G, Chiorean E, Fishman M, Saboury B, Teitelbaum U, Sun W, et al. CD40 agonists alter tumor stroma and show efficacy against pancreatic carcinoma in mice and humans. Science 2011;331:1612–6.
23. Pyonteck SM, Akkari L, Schuhmacher AJ, Bowman RL, Sevenich L, Quail DF, et al. CSF-1R inhibition alters macrophage polarization and blocks glioma progression. Nat Med 2013;19:1264–72.
24. Ries CH, Cannarile MA, Hoves S, Benz J, Wartha K, Runza V, et al. Targeting tumor-associated macrophages with anti-CSF-1R antibody reveals a strategy for cancer therapy. Cancer Cell 2014;25:846–59.
25. Kaneda M, Messer K, Ralainirina N, Li H, Leem C, Gorjestani S, et al. PI3Kγ is a molecular switch that controls immune suppression. Nature 2016;539: 437–42.
26. Holmgaard RB, Brachfeld A, Gasmi B, Jones DR, Mattar M, Doman T, et al. Timing of CSF-1/CSF-1R signaling blockade is critical to improving responses to CTLA-4 based immunotherapy. Oncoimmunology 2016;5: e1151595.
27. Hoves S, Ooi C-H, Wolter C, Sade H, Bissinger S, Schmittnaegel M, et al. Rapid activation of tumor-associated macrophages boosts preexisting tumor immunity. J Exp Med 2018;215:859–76.
28. Perry C, Muñoz-Rojas A, Meeth K, Kellman L, Amezquita R, Thakral D, et al. Myeloid-targeted immunotherapies act in synergy to induce inflammation and antitumor immunity. J Exp Med 2018;215:877.
29. Sharma P, Allison J. The future of immune checkpoint therapy. Science 2015;348:56–61.
30. Brahmer J, Tykodi S, Chow L, Hwu W-J, Topalian S, Hwu P, et al. Safety and activity of anti–PD-L1 antibody in patients with advanced cancer. N Engl J Med 2012;366:2455–65.
31. Powles T, Eder JP, Fine GD, Braiteh FS, Loriot Y, Cruz C, et al. MPDL3280A (anti-PD-L1) treatment leads to clinical activity in metastatic bladder cancer. Nature 2014;515:558–62.
32. Pauken K, Sammons M, Odorizzi P, Manne S, Godec J, Khan O, et al. Epigenetic stability of exhausted T cells limits durability of reinvigoration by PD-1 blockade. Science 2016;354:1160–65.
33. Huang A, Postow M, Orlowski R, Mick R, Bengsch B, Manne S, et al. T-cell invigoration to tumour burden ratio associated with anti-PD-1 response. Nature 2017;545:60–65.
34. Sen D, Kaminski J, Barnitz R, Kurachi M, Gerdemann U, Yates K, et al. The epigenetic landscape of T cell exhaustion. Science 2016;354: 1165–69.
35. Le DT, Durham JN, Smith KN, Wang H, Bartlett BR, Aulakh LK, et al. Mismatch-repair deficiency predicts response of solid tumors to PD-1 blockade. Science 2017;357:409–13.
36. Herbst RS, Soria J-CC, Kowanetz M, Fine GD, Hamid O, Gordon MS, et al. Predictive correlates of response to the anti-PD-L1 antibody MPDL3280A in cancer patients. Nature 2014;515:563–7.
37. Gubin MM, Esaulova E, Ward JP, Malkova ON, Runci D, Wong P, et al. High-dimensional analysis delineates myeloid and lymphoid compartment remodeling during successful immune-checkpoint cancer therapy. Cell 2018;175:1014–30.
38. Love M, Huber W, Anders S. Moderated estimation of fold change and dispersion for RNA-seq data with DESeq2. Genome Biol 2014;15: 550.
39. Ritchie M, Phipson B, Wu D, Hu Y, Law C, Shi W, et al. limma powers differential expression analyses for RNA-sequencing and microarray studies. Nucleic Acids Res 2015;43:e47.
40. Subramanian A, Tamayo P, Mootha VK, Mukherjee S, Ebert BL, Gillette MA, et al. Gene set enrichment analysis: a knowledge-based approach for interpreting genome-wide expression profiles. Proc Natl Acad Sci USA 2005;102:15545–50.
41. Wu D, Smyth G. Camera: a competitive gene set test accounting for inter-gene correlation. Nucleic Acids Res 2012;40:e133.
42. Duluc D, Corvaisier M, Blanchard S, Catala L, Descamps P, Gamelin E, et al. Interferon-gamma reverses the immunosuppressive and protumoral properties and prevents the generation of human tumor-associated macrophages. Int J Cancer 2009;125:367–73.